Mechanism for Determination of G-factors for Solid Freeform Fabrication Techniques Based on Large Heat Input

Rajeev Dwivedi, Srdja Zekovic, Radovan Kovacevic
Research Center for Advanced Manufacturing
Southern Methodist University, 1500 International Parkway Suite 100

Richardson, TX 75081

Abstract

A major class of Solid Freeform Fabrication (SFF) methods for metal deposition are based on large heat input. The geometry and microstructural properties of the deposition depend primarily on the heat input and the subsequent distribution at the substrate. On one hand the insufficient heat may lead to the inadequate melting of the metal, on the other hand overheating and heat accumulation leads to the over-melting, resulting in the deformation of the build up geometry. The heat distribution is governed by the available heat sink . For a better control of the process, the estimation of heat sinks and the subsequent control of the energy input allows a better control of the process. A parameter G-factor that estimates the heat sink based on the local geometry of a part has been introduced. The estimation of G-factor is based on the simulation and the experimental results. Also a mechanism to determine the G-factor for various substrate geometries has been introduced.

1 Introduction

Recently, the Laser assisted metal deposition for the Solid Freeform Fabrication (SFF) of the functional parts has become very popular. Laser-based Direct Metal Deposition (LB-DMD) is one of the laser assisted metal deposition techniques which can build full density metal components directly from CAD files. LBDMD is a segment of MultiFab system under development at RCAM, Southern Methodist University, which integrates additive and subtractive manufacturing technologies. The fundamental scheme of LBDMD as described in Fig. 1 includes the delivery of metal powder in a molten pool formed by focusing a continuous wave multi mode Nd:YAG laser onto a metallic substrate. An inert gas such as Argon acts as the carrier medium for the metal powder. The metal powder melts and adheres to the substrate or the underlying deposit. The dimensions of the deposition depend on the

size of the molten pool. A desired geometry is obtained by the relative spatial motion of the substrate and the metal deposition head.
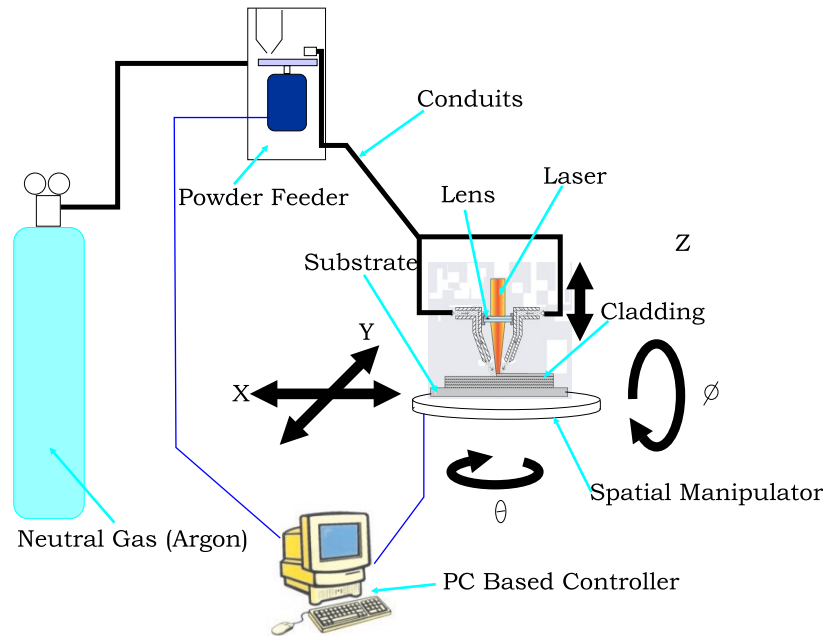

Fig. 1: System for Laser Based Direct Metal Deposition

The accuracy of the feature geometry, desired microstructure and development of the residual stresses depend on the heat input. The heat management in the process is extremely complex. The complexity of heat management is a result of the involvement of a number of parameters such as:

1. Heat Input.

2. Material properties of the substrate and added material.

3. The speed and convective properties of the carrier gas.

4. The relative motion of the substrate with respect to the heat source.

5. The instantaneous geometry of the heat sink.

Uncontrolled process parameters may result in the inconsistent geometry of the molten pool. One of the possible solutions to this is the use of a feedback control based on the image of the molten pool [1]. However, the speed of the process and the time lags associated with the acquisition of the molten pool image, the time required for the information extraction and sending control signals, and finally the time required for the stability of the laser power does not allow the implementation of feedback control for the process. The most effective way to get a good quality deposition, therefore, is to estimate the relevant parameters using a

suitable approach such as simulation and experimentation followed by direct implementation of a feed-forward control.

Aspects of the LBDMD that depend on the heat transfer may be listed down as:

- microstructure

- geometry

- residual stresses

The rate at which heat transfer takes place across the liquid-solid phase boundary, determines the microstructure of the part. The geometry of deposition depends on the size of the molten pool, that in turn depends on the heat transfer conditions. The heat transfer conditions at the substrate as well as already deposited material and the immediate vicinity of the molten pool determine the temperature distribution in the buildups. The temperature distribution in the buildups determines the development of residual stresses in the deposition.

A vast amount of work has been done towards the simulation of the LBDMD process in the past [1–5]. However, most of the work has been confined to the two-dimensional analysis or the analysis of thin wall structures. We investigate in this work the influence of varied bulk substrate geometry on the deposition.

As described earlier, the size of the molten pool is outcome of a very complex interaction of a variety of process parameters. In order to solve the problem, a set of simulations and experiments are performed. For a given set of process parameters, the underlying heat sink geometry is varied. Finally the size of the molten pool, determined experimentally and using the simulation is compared.

The work also borrows the fundamental idea of the Geometrical Factors (G-factors) introduced by Kmecko et. al [6, 7] to quantify the heat sink towards the process planning. The basic mechanism used to determine the G-factors is based on the principles of geometric modeling.

The results obtained are used to develop an analytical model towards the process planning and determine the parameters for feed-forward control of the process.

2   The SFF Process Model

A solid S defined in a 3-D Eucledian space is a closed subset of R^3 such that it is identified by its *interior* defined as $p \in S$ and its exterior, $p \notin S$, is the complement . The boundary of the solid is defined by the region $p \in \partial S \subset S$ that is the subset of solid where any neighborhood contains non-members.

The solid fabricated by the SFF exhibits a near uniform cross-section over each layer. A mathematical model for the layer can be described as the sweep of the area A along the vector $\hat{v}_g$ where the subscript g corresponds to the growth direction. Let us define the fabrication of the part by SFF as a set of entities *swept* along a growth direction.

$$P = \bigcup_{i=1}^{n} A_i \oplus \hat{v}_g \tag{1}$$

where $\oplus$ represents the Minkowski sum and $A_i \oplus \hat{v}_g$ is the translation of ith cross-section A_i along the vector $\hat{v}_g$.

For the thermal model; however, the model should be able to take into account the transient component. The addition of subsequent layers accounts for the varying heat sink over the time. The geometric model, therefore, is modified to:

$$P(l) = \bigcup_{i=0}^{l-1} A_i \oplus \hat{v}_g \tag{2}$$

where $P(l)$ corresponds to the substrate available for the fabrication of lth layer. For the bulk geometry, we use variants of the semi-infinite body.

For a solid S, at a given instant, the geometry of the molten pool is expressed by a time varying scalar field $F(t) : R^3 \rightarrow R(t)$ such that the set of points $p(x, y, z) \in S$ satisfy:

$$F(p, t) = \begin{cases} \text{True} & T(p, t) \geq T_m \\ \text{False} & T(p, t) < T_m \end{cases} \tag{3}$$

where T_m is the melting temperature of the substrate material. Correspondingly, the shape factor $\eta(p)$ of a geometric location is the ratio of the instantaneous volume of the molten pool and the molten pool for a perfect semi-infinite body geometry for the given power source.

$$\eta(p) = \frac{Vol(F(p))}{Vol_{max}} \tag{4}$$
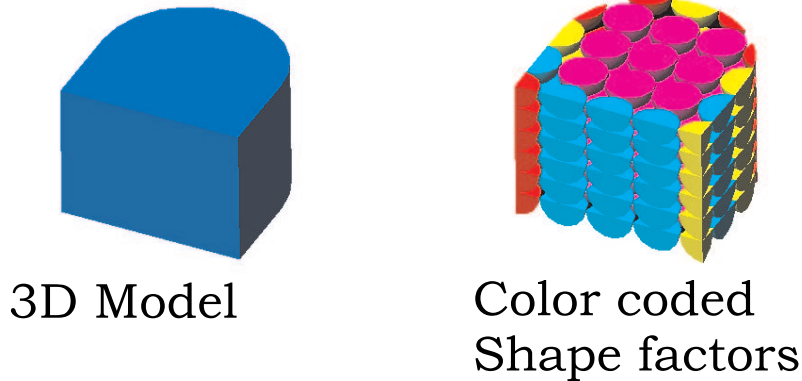

3D Model   Color coded Shape factors

Fig. 2: A 3D model and its corresponding color coded shape factor

The molten pool for a perfect semi-infinite geometry is hemispherical [6,7]. The radius of the hemisphere is a characteristic of the set of process parameters including the heat source the material thermal properties and the ambient heat transfer conditions. The mechanism to determine the shape factor of a point is expressed by the following relationship:

$$\eta(p) = \frac{Vol(HemSph(p) \bigcap SolidM(p))}{Vol_{max}} \quad (5)$$

where the $HemSph(p)$ is the solid model geometry of a hemi-sphere at the given location p, $SolidM(p)$ is the geometry of the solid model under investigation and $\bigcap$ is the Boolean operation between two solid entities.

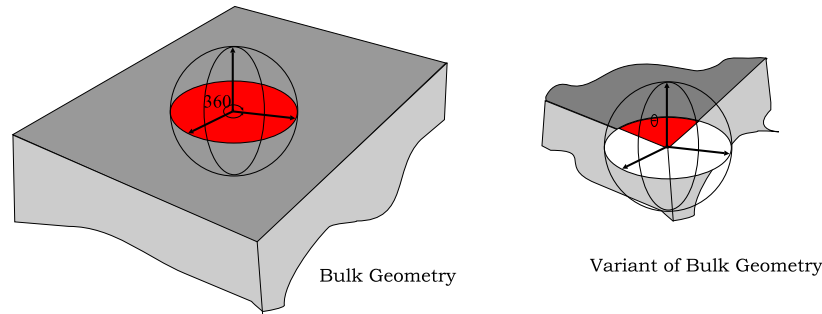Fig. 2 describes a model and the corresponding color coded shape factors at different locations.

Fig. 3: Characterization of geometry by angle

A trivial observation suggests that the geometry of immediate substrate can be characterized by an angle. As shown in the Fig. 3, the characterizing angle for a point on the bulk is 360°. Similarly an angle θ can be attributed to the variant of a bulk geometry. Owing to the inherent property of conductive heat transfer in isotropic metal bulk Vol_{max} can be characterized by 360° similarly the parameter $Vol(F(p))$ can be characterized by θ, where θ is the angle that defines the geometry.

However, the heat transfer conditions are nonlinear due to involvement of the radiative and convective mode therefore a more detailed investigation is required. The heat source is simplified as a uniform flux circular area. The details of the heat input is described in detail in the later sections .

3   Development of the Heat Transfer Model

3.1   Geometry of Solid Used for Simulation

The physical model used for the simulation and experimentation in essence captures the geometry of a variety of heat sinks. The top face of the geometry represents variants of semi-infinite geometry. The geometries include corners that provide heat sinks with a range

Table 1: The points under consideration, order of visit and the shape factors

Visit Order Number	Characterizing angle (in degrees)	Shape Factor
4	45	0.125
2	90	0.25
3	135	0.375
7	180	0.5
5	270	0.75
8	360	1

of characterization angles. The characterization angles included in the geometry are 45°, 90°, 135°, 180°, 270° and 360°. The order of the dimensions of the part is much higher than the size of molten pool such that the influence of the overall geometry of the part can be ignored when compared to the heat transfer for the local heat sink geometry.
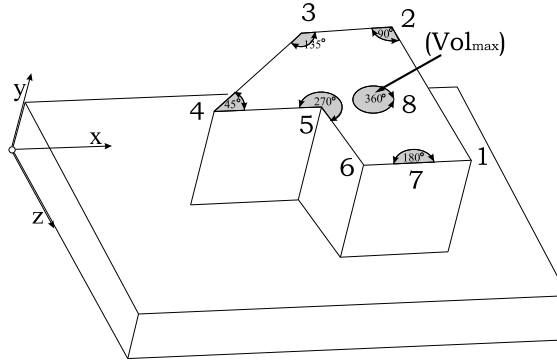

Fig. 4: The 3D model and the heat sinks for different geometries

The model of the substrate geometry is shown in Fig. 4. The order of visit of the corners that the heat source follows is shown in the fig ($1 \rightarrow 2 \rightarrow 3 \rightarrow 4 \rightarrow 5 \rightarrow 6 \rightarrow 7 \rightarrow 8$). Corners 1, 2 and 6 represent the heat sink corresponding to the characterizing angle 90°, therefore, the point chosen for the investigation is 2. The order of corners, characterizing angle and the corresponding shape factors are elaborated in the table 1.

3.2 Governing Equations

The foremost concern in the analysis is the modeling of the heat transfer and temperature history; therefore, the development of residual stresses and corresponding deformations are neglected. Also, the thermo-physical properties of deposited material are assumed to be uniform and isotropic. The transient model of the heat transfer equation is given by:

$$k(\frac{\partial^2 T}{\partial x^2} + \frac{\partial^2 T}{\partial y^2} + \frac{\partial^2 T}{\partial z^2}) + Q(x,y,z,t) = \rho c(\frac{\partial T}{\partial t} - v\frac{\partial T}{\partial x}) \tag{6}$$

375

where (x, y, z) corresponds to the coordinates, t is the time, T is the temperature, $Q(x, y, z, t)$ is the heat content of the system as a function of time. c is the specific heat, ρ is the material density and k is the thermal conductivity.
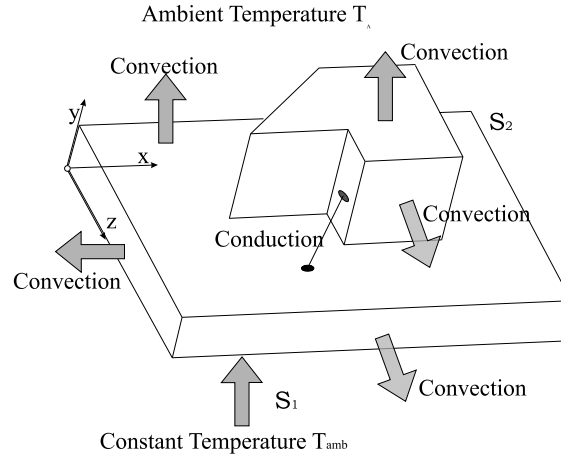

Fig. 5: Boundary conditions applied to the model

The set of boundary conditions and the affiliation of the geometry to the boundary conditions is described in Fig. 5.

The essential boundary condition is defined as:

$$T(x, y, z, 0) = T_{amb}(x, y, z, t) \tag{7}$$

where T_{amb} is the ambient temperature being applied to the boundary $(x, y, z) \in S_1$, representing the bottom surface of the substrate for $t > 0$ (Fig. 5). The boundary condition can be applied safely because size of the substrate is large enough compared to the size of build up and the substrate is cooled by a cooling plate. The natural boundary condition is expressed as:

$$k_n \frac{\partial T}{\partial n} + Q + h(T - T_{amb}) + \sigma \varepsilon (T^4 - T_{amb}^4) = 0 \tag{8}$$

where k_n is the thermal conductivity along the normal to the surface, Q is the heat flux normal to the surface, h is the convection heat transfer coefficient, σ is the Stefan-Boltzmann constant for radiation and ε is the surface emissivity.

The natural boundary condition is applied to the boundary $(x, y, z) \in S_2$ corresponding to the surfaces subjected to heat transfer by radiation, convection and the heat fluxes for $t > 0$ (Fig. 5).

The initial condition is described as:

$$T(x, y, z, 0) = T_0(x, y, z) \tag{9}$$

The above described material properties are; however, dependent on the temperature; therefore, they must be incorporated in the model. The inclusion of the temperature dependent thermo-physical properties and the parameters corresponding to the radiation make the analysis highly nonlinear. For the simulation purposes, certain simplifications to the model are introduced. The radiative heat transfer has shown a difference of as much as 3 percent, when compared to the solution with ignored radiation [5]. We incorporate; therefore, an empirical relationship proposed by Vinakurov et. al [8] for the simplification:

$$h = 2.4 \times 10^{-3} \varepsilon T^{1.61} \tag{10}$$

The Eq. 10 suggests a modified convection heat transfer coefficient that combines the effect of radiation and convection. The corresponding accuracy losses are estimated to be less than 5 per cent [8].

4   Assumptions and the Problem Definition

It is not feasible to incorporate the exact details of the process for the modeling purpose however certain assumptions are made to simplify the modeling process in order to get near accurate simulation of the model. The assumptions made are:

- The workpiece is initially at the room temperature (298 K)

- Thermo-physical properties are temperature dependent and are borrowed from the data provided by [9] and [10]. The values for higher range of temperatures and phase transforms are based on experimental data, relationships and extrapolation schemes suggested in [11–15].

- The input power from the power source remains invariant over the process. In reality there might be slight fluctuations in the power delivered by the laser.

- The intensity variation of the beam emanating from the optical fiber is uniform.

- The heat flux input used is based on the mean uniform distribution of the thermal flux over the area given by:
$$I_m = \frac{0.865AP}{\pi r_b^2} \tag{11}$$

  Where A is the absorptivity. For the material(H13-tool steel) and the temperature ranges used in the simulations and the experiment, the value used is 0.35 [2]. r_b is the effective laser beam radius.

- The body undergoes a uniform forced convection and the effect of gas diffusion is ignored.

- The surface-to-surface contact between the workpiece and the support plate is ideal, such that the mode of heat transfer is conduction.

- The latent heat of fusion is based on the analytic relationship provided by Brown and Song [16] given by:

$$H = \int \rho c(T) dT \qquad (12)$$

- The convective redistribution of temperature in the molten pool, for the LBDMD is ignorable due to rapid melting and solidification. Also for all the power and the temperature ranges of simulations and the experiments, the heat loss due to evaporation can be ignored [2].

A commercially available software, $ANSYS^{TM}$ has been used for the modeling and simulation of the process. $ANSYS^{TM}$ parametric design language (ADPL) is used to develop a code for the time dependent location of the heat flux boundary condition. The discretized FEM model is based on the 3D thermal solid element. The basic properties of the element include eight nodes with single degree of freedom and temperature at each node. The consistency of the heat flux during the deposition is maintained through iteration.

5 Simulation and Experimental Verification

Table 2: The process parameters used for the experiments

Parameter	Value
Power	350W
Speed	5 mm/s
Gas Flow	12 cu-ft/hr

The FEM simulation and the experiment are based on the set of parameters described in Table 2. The laser head with specified set of parameters is traversed over the contour of a block with the geometry described in Fig. 4. After the deposition is done, the block is cross cut, polished and the molten pool at different corners is identified. The Cross-sectional area of the molten pool obtained experimentally is presented in Fig. 6.

Table 3: The volume of the molten pool obtained by experiment and simulation

Characterizing Angle	Simulation (mm^3)	Experiment (mm^3)
45	1.899	3.804
90	1.831	2.27
135	1.726	2.25
180	1.23	1.77
270	1.13	1.22
360	0.8443	0.47

For the simulation, the size of the molten pool is identified by the relationship described in Eq. 3. The size of the molten pool at different corners of the substrate determined experimentally and by simulation is shown in the Table 3.
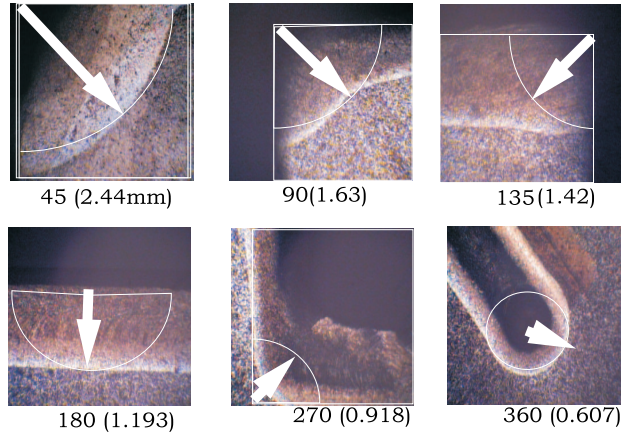

45 (2.44mm)   90(1.63)   135(1.42)

180 (1.193)   270 (0.918)   360 (0.607)

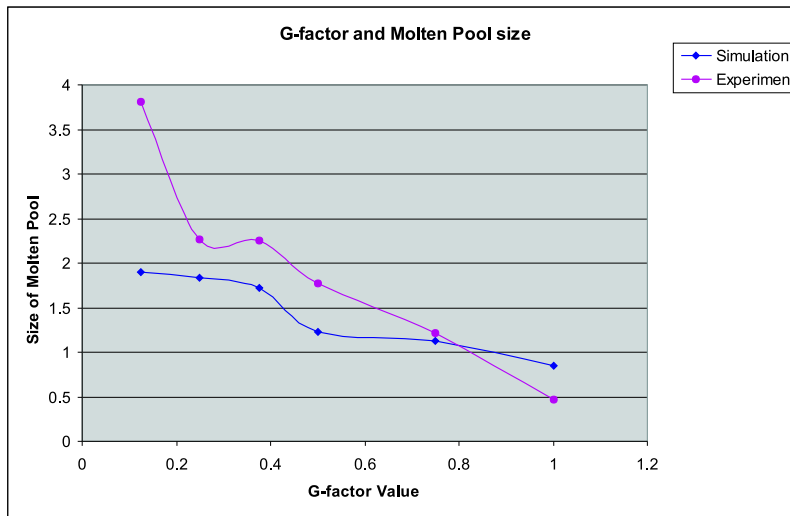Fig. 6: The radius of molten pool obtained experimentally

Fig. 7: The correlation between the volume of molten pool obtained experimentally and by simulation

Fig. 7 describes the relationship between the size of the molten pool and the shape factor of the substrate geometry obtained by numerical simulation and experimentally.

It is observed that for most of the range of geometries the experimental and simulation results are in a good agreement. Fig. 8 show a pictorial and 3D view of the molten pool for different substrate geometries as obtained by simulation.
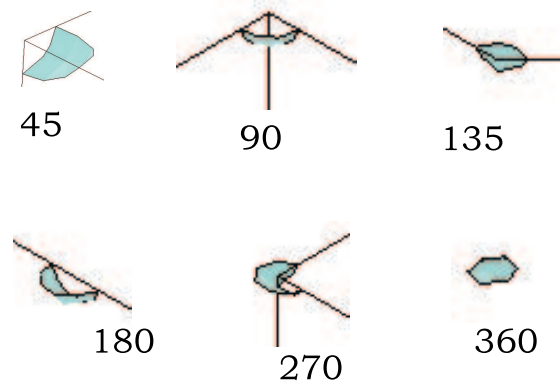
Fig. 8: The relative size of molten pools -3D

6 Conclusions

A substrate having a variety of geometry was identified. Experiment and the simulation to determine the size of the molten pool was performed. A relationship between the G-factor of the geometries and the size of the molten pool is derived. It is observed that there exists a strong relationship between the size of the molten pool and the shape factor. A suitable approach to determine the shape factor of geometries is also suggested. The correlation derived between G-factors and size of molten pool can be used to adjust the heat input for a consistent size of molten pool.

The future work includes development of a feedforward controller and implementation algorithm in order to have a consistent molten pool size and heat gradient during laser based metal deposition.

Acknowledgment

References

[1] D. Hu and R. Kovacevic. Sensing, modeling and control for laser-based additive manufacturing. *The International Journal of Machine Tools and Manufacture*, 43:51–60, 2003.

[2] A.J.Pinkerton and L. Li. An analytical model of energy distribution in laser direct metal deposition. *Proceedings of the I MECH E Part B Journal of Engineering Manufacture*, 218(4):363–374, April 2004.

[3] O. O. Neto. Diniz. Physical-computational model to describe the interaction between a laser beam and a powder jet in laser surface processing. *Journal of Laser Applications*, 14(1):46–51, February 2002.

[4] Toyserkani Ehsan. *Modeling and Control of Laser Cladding by Powder Injection*. PhD thesis, University of Waterloo, 2003.

[5] D. Hu D. and R. Kovacevic. Modeling and measuring the thermal behaviour of the molten pool in closed-loop controlled laser-based additive manufacturing. *Proceedings of Institution of Mechanical Engineers, Part: Journal of Engineering Manufacture*, 217:441–452, 2003.

[6] I. Kmecko, Z. Jandric, and R. Kovacevic. Influence of geometric factor on heat transfer rate during gtaw for rapid prototyping. In *(2001) Proceedings of the symposium on Nontraditional Manufacturing Research and Applications, International Mechanical Engineering Congress and Exposition*, New York, NY, Nov 11-16 2001.

[7] Z. Jandric. *Optimization of Hybrid Rapid Manufacturing/Repair Process*. PhD thesis, Southern Methodist University, May 2003.

[8] V. A. Vinakurov. *Welding Stresses and Distortion*. Boston Spa, London, 1987.

[9] http://www.moldsteel.com/h13.htm. International mold steel inc, premium h13.

[10] *ANSYS Theory Manual, Release 8.1*. ANSYS, Inc., USA, 2004.

[11] Dieter Radaj. *Heat Effects of Welding ; Temperature Field, Residual Stresses, Distortion*. Springer-Verlag, 1992.

[12] J A Goldak, M J Bibby, J E Moore, R House, and B Patel. Computer modelling of heat flow in welds. *Metallurgical Transactions B.*, 17B(3):587–600, September 1986.

[13] Ed. in Chief John F. Ready. *LIA Handbook of Laser Materials Processing*. Laser Institute of America, 2001.

[14] J A Goldak, A Chakravarti, and M J Bibby. A new finite element model for welding heat sources. *Metallurgical Transactions B.*, 15B(2):299–305, June 1984.

[15] J H Argyris, J. Szimmat, and K J William. Finite element analysis of arc-welding process. *Numerical methods in heat transfer*, 3, 1985.

[16] S Brown and H Song. Finite element simulation of welding of large structures. *Transactions of ASME*, 114(4):441–451, 1992.